

Article

Simulation of Phase Change Material Absorbers for Passive Cooling of Solar Systems

Abdelhakim Hassabou¹ and Rima J. Isaifan^{2,*} 

¹ Department of Renewable Energy, Cambridge Corporate University, Seeburgstrasse 20, 6006 Luzern, Switzerland

² Division of Sustainable Development (DSD), Hamad Bin Khalifa University (HBKU), Education City, Doha P.O. Box 5825, Qatar

* Correspondence: risaifan@hbku.edu.qa

Abstract: One of the main challenges that face the reliable use of photovoltaic solar systems in hot arid regions is the prevailing high temperatures during the day. To overcome this issue, Phase Change Materials (PCM) are used for passive cooling providing different options to attain sufficient thermal management solutions for different applications. Passive cooling can be achieved by adjusting a heat sink to the solar PV module. This can be realized by attaching a PCM layer or sensible heat storage to the backside of PV panels. Few studies have reported on simplified modeling and numerical procedures using the apparent heat capacity formulation and volume averaging technique as a robust approach to solving such sophisticated problems with minimal computational efforts, high accuracy, and in a short period of time. However, there is still a need to bridge the large-scale gap between the macroscale within the PCM layer, with a moving melting front, and the length scale of PV modules. Hence, this work focuses on modeling and simulating PCM-Matrix Absorbers (PCM-MA) that consist of fibrous aluminum cellular structure filled with PCM for passive thermal management of PV panels using apparent heat capacity formulation and homogenization based on volume averaging technique. COMSOL Multiphysics FEM software was used for the numerical simulation of the phase change problem by using a Smoothed Heaviside step function to overcome the singularity of PCM challenge that arises with sharp melting temperatures. To validate the proposed model, it has been compared with a benchmark analytical solution for an ice melting problem, i.e., the Stefan problem, in a semi-finite slab, i.e., Neumann's solution under the same assumptions and boundary conditions. The specific characteristics of phase change and evolution of melting front with time, heat capacity change with the temperature at different times, and with locations along the slab height are presented. As the phase change is modeled to take place over a mushy region, i.e., a narrow temperature interval rather than a sharp melting point, the results show a good coincidence of the heat capacity profile and its peak at different times and locations. The validated model can be used for the optimization of PCM-MA for any specific geographical location and other applications such as the passive cooling of buildings with PCM integrated with the outer envelope. To this end, the results of the simulation in this work are shown to be in agreement with those obtained from the analytical solution.

Keywords: solar power; solar PV efficiency; passive cooling; PCM; thermal management; thermal energy storage



Citation: Hassabou, A.; Isaifan, R.J. Simulation of Phase Change Material Absorbers for Passive Cooling of Solar Systems. *Energies* **2022**, *15*, 9288. <https://doi.org/10.3390/en15249288>

Academic Editor: Karunesh Kant

Received: 30 October 2022

Accepted: 20 November 2022

Published: 7 December 2022

Publisher's Note: MDPI stays neutral with regard to jurisdictional claims in published maps and institutional affiliations.



Copyright: © 2022 by the authors. Licensee MDPI, Basel, Switzerland. This article is an open access article distributed under the terms and conditions of the Creative Commons Attribution (CC BY) license (<https://creativecommons.org/licenses/by/4.0/>).

1. Introduction

The operation of solar photovoltaic (PV) systems in hot climatic areas where extremely high temperature and humidity conditions prevail is a major challenge in the field [1–3]. More specifically, the efficient operation of PV systems requires a reliable thermal management tool to sustain the power output and increase the life expectancy of the panels.

The efficiency of PV cells is proven to drop significantly at high temperatures when the cooling demand is also high. This indicates that maintaining the temperature of PV

modules at a lower level is highly desirable. In hot climates, air cooling with natural convection would be less effective, hence active thermal management of PV cells becomes a necessity. While cooling of PV modules is only needed during the daytime, air humidity condensation on PV panels should be avoided during both day and nighttime. This prevents mud formation in the existence of dust which would start if the temperature of the module surface falls below the dew point. Mud formation on the module surface increases maintenance cost, shortens the module's lifespan, and decreases its efficiency in addition to the high-temperature adverse effects. To address this issue, the active thermal management of PV modules using hybrid photovoltaic-thermal (PV/T) solar collectors, that generate both heat and electricity from the solar resource, is of special interest. One of the important advantages of PV/T systems is the simultaneous generation of electrical and thermal energy in the same collector, with no additional land footprint. Thus PV/T can be more cost effective than PV and solar thermal collectors standing alone, especially for applications that require both electricity and hot water at relatively low temperatures.

Kern and Russell initially reported on the hybrid PV/T solar collectors [4] which was followed by other studies [5,6]. Many practical applications of PV/T were reviewed including several design options such as different types of PV cells (e.g., monocrystalline, polycrystalline, thin film), concentrating or non-concentrating flat plate collectors, glazed or unglazed, natural or forced flow, standing alone or building-integrated Zhang et al. [7].

A diversity of PV/T system designs has been developed with focus on two main applications: where two different applications: obtaining electricity at improved conversion efficiency of PV panels with low temperature of the heat transfer fluid (HTF) or sacrificing the electrical efficiency for obtaining HTF at higher temperature. In the first arrangement, unglazed cheap collectors can be used as the HTF temperature is controlled below 40 °C. In the second arrangement, HTF temperatures above 60 °C are usually desired. Consequently, higher cell temperatures will lead to a decrease in both electrical and thermal efficiencies. Additional glazing and thermal insulation of the collector suppresses thermal losses of the collector and improve the thermal efficiency, at the expense of electrical efficiency.

While PV/T collectors in the moderate climatic zones like in Central Europe are in competition with the falling PV module prices, the use of PV/T still can be of advantage in hot arid climate regions. However, due to the involvement of a relatively high level of process engineering with water piping and circulation pumps as well as related engineering costs of the PV/T systems, it may not be suitable for small and medium scale applications or remote isolated areas in deserts.

Therefore, one thermal management process that meets the demand in such hot areas is passive cooling [8]. Passive cooling utilizes the tangible difference in temperature during day and night in hot areas. The passive cooling materials (PCM) are characterized by the high thermal capacity that maintains PV cells at an acceptable temperature during the day by accumulating coolness during the night. The thermal energy accumulated during daytime in the PCM layer is released gradually to the ambient during nighttime. The gradual discharge of accumulated heat keeps the PV panel temperature above the dew point of the surrounding air to prevent condensation during the night. This, in turn, minimizes the chance for mud to form which causes cementation of dust on the panel surface [2,9]. The latter effect can reduce water consumption and mechanical efforts in the cleaning of PV modules in deserts and dusty regions.

However, one of the main drawbacks of PCM that adversely impacts charging and discharging processes by limiting PV power density is the low thermal conductivity. Therefore, several studies have proposed the application of metal fibers to enhance the PCM absorber thermal conductivity [1,10,11]. Consequently, an increasing attention has been paid to using PCM in thermal management of PV modules in the last few decades with considerable research and scientific analysis conducted to enhance the knowledge in this field both experimentally and numerically. Choubineha et al. experimentally examined the effect of both natural and forced air convection cooling of PV modules equipped with PCM on the modules' electrical efficiency [12]. The results showed that using PCM layers

with 6 mm thickness led to reducing the panel temperature under different natural and forced convection modes which led to an increase in the output power and electrical efficiency. Moreover, Adibpoura et al. examined the effect of PCM cooling on a tracking PV module [13]. The results showed that the melting dynamics of PCM is very different while tracking compared to previous research on fixed panels. More specifically, the efficiency of tracking PV modules with PCM is on average 4.6% higher than that without PCM. Hassabou et al. have performed comprehensive experimental analysis on PV passive cooling with PCM under hot weather conditions for nine months in Qatar using one type of Monocrystalline PV modules and two PCM absorber thicknesses of 30 mm and 50 mm, and a melting point of 54 °C [1]. The experimental analysis showed that the PV module's peak temperature was shaved by 10 °C with the PCM effect compared to reference PV modules without PCM.

However, the simulation of such set up encounters sophisticated challenges in coupling the physics of phase change phenomena with a moving melting and solidification fronts at the macroscale level with the length scale of PV modules. This scale gap imposes some limitations on the number of simulation cases in the open literature. Other difficulties involved in modelling the PCM layer include the consideration of internal convection heat transfer effects, accurately tracking the moving boundary that is neither desirable nor easy due to the scale gap and the impact of some common assumptions in numerical simulation on the accuracy of the model.

The main focus of this work is to develop a simplified, yet robust numerical simulation tool, that can be used to solve such sophisticated phase change problems inside the PCM layer with minimal computational efforts, high accuracy and in a short period of time. This simplified and accurate model is extremely important to bridge the big scale gap between the macroscale level within the PCM layer with moving melting front/solidification and the length scale of PV modules, without the need to track the moving boundary.

2. Methods

2.1. Approaches for Modelling Solid-Liquid Phase Change

The transient non-linearity phenomenon in the heat transfer in PCM is coupled with a moving solid-liquid interface. This moving boundary is normally presented as the “moving boundary” or “Stefan” problem [14]. The challenge, in this case, is generally associated with the uncertainty of the PCM physical properties as well as not having enough details about the natural convection in the liquid phase. The two main heat transfer modes during the melting and solidification process in this configuration are mainly conduction, and to a less extent, natural convection due to the temperature difference that exists in the liquid-solid interface. Nevertheless, the effect of natural convection can be neglected in the solid-liquid interface compared with the heat conduction in the solid PCM [15]. Figure 1 shows the integration of PCM as a heat sink with solar PV modules.

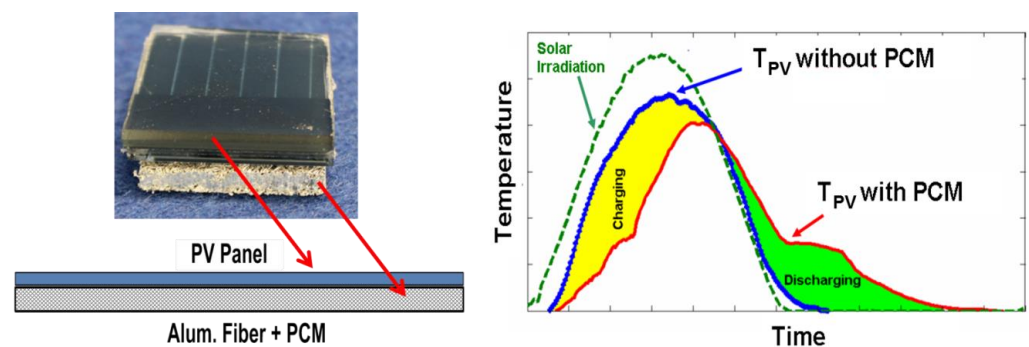


Figure 1. Passively cooled solar PV panel: (Left) photographic and schematic view of a cross-sectional sample of PV panel with PCM matrix absorber, and (right) illustration of day and night heat absorption (charging) and release (discharging); respectively.

2.1.1. Analytical Methods

Several analytical methods for solving moving boundary surface problems were reviewed by Mori and Araki [16]. It should be stressed that few exact analytical solutions are available, and those that do exist are primarily for one-dimensional (1-D) problems. Generally, the set of partial differential equations describing the heat transfer of the latent heat energy storage systems is not solved analytically due to nonlinearity as well as the presence of complicated boundaries.

One of the most precise and well-known analytical solutions for Stefan's problem related to the one-dimensional moving boundary nature of the problem was proposed by Neumann [14]. In the analytical solution, it is assumed that the melting temperature or (solidification temperature when prevails) is constant, which is not the dominant case in many phase change mediums. Therefore, the use of numerical methods shall be investigated to provide sufficiently accurate solutions and identify configurations of particular interest.

2.1.2. Numerical Methods

Several different numerical methods were proposed to solve problems that involve continuously moving phase change boundary at a specific temperature or narrow temperature range. Voller has extensively reviewed these methods where he grouped them into three categories: fixed-domain, front-fixing, and front-tracking strategies [17]. Moreover, three methods have been further proposed to solve the fixed-domain ones which are the enthalpy, temperature, and the apparent heat capacity methods.

The enthalpy method considers that enthalpy is the only control variable and expresses temperature as a function of enthalpy, then the enthalpy-temperature relation is introduced into the formulation to eliminate the temperature from the governing equations. The interface is eliminated from consideration in the calculations and the problem is reduced to heat conduction without phase change. This method can be applied to the whole domain regardless of the phase at a certain point which eliminates the need to track the phase change interface, which becomes unnecessary. Hence, when the enthalpy method is used, the temperature field needs to be evaluated as a function of the enthalpy, since enthalpy is taken as the control variable over the entire grid. In this case, the reference point of enthalpy is selected as zero degrees Celsius, and the thermodynamic enthalpy-temperature relation of the PCM is called the constitutive equation. By introducing the constitutive equation into the formulation, the temperature can be eliminated from the governing equations. Therefore, the interface is eliminated from consideration in the calculations. Hence, this waives the need to consider sides or the region of the interface separately. Moreover, no additional condition at the interface melting front shall be satisfied. As a result, the two-phase moving boundary problem becomes a normal heat conduction problem without phase transition. In addition, the phase change problems are easier to solve numerically by making use of the enthalpy-based method. Nevertheless, for a pure PCM, the temperature is a unique function of enthalpy which provides the singularity aspect to the problem.

In the temperature method, the temperature is the control variable, and the enthalpy is the dependent variable. The simulation of the phase change phenomenon needs the solution of the conservation equations considering separately both the convection and conduction in the liquid (melt) zone and the conduction in the solid zone. Moreover, in order to couple both phases (liquid and solid) together, an interface equation is needed. Obviously, the melting front needs to be instantaneously tracked in this method.

In the apparent heat capacity method to solve heat conduction problems with phase change, the temperature becomes the primary dependent variable to be derived from the solution. Hence; it is assumed that the phase change takes place at a fixed temperature or over a small temperature interval [18]. This method has been developed by Civan and Sliepcevic and shall be utilized in this work for semi-infinite media [18].

The following section provides the background formulation of the general problem for the apparent heat capacity method, and special techniques for the solution are presented in the following section. The Neumann analytical solution for ice melting in a semi-finite slab

heated from below and isolated from other sides will be presented for the sake of validation of the numerical simulation based on the apparent heat capacity method.

2.2. Numerical Solutions of Solid-Liquid Phase Change Problems

2.2.1. Background on Stefan's Problem

This problem concerns the numerical simulation of melting and solidification inside a slab involving a moving boundary. The classically called "Stefan problem" is shown in Figure 2.

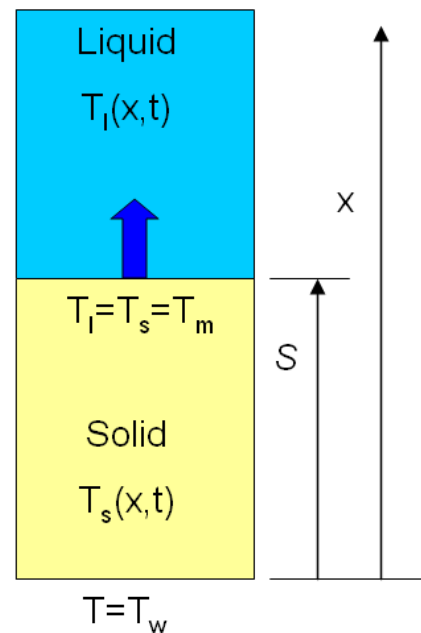


Figure 2. Ice freezing with a moving solidification front.

The physical problem states that a liquid solution is initially cooled to below the solidification/melting point which causes an ice front formation that moves in space and time across the domain as shown in Figure 3. In order to describe the transient heat transfer with phase change in the domain that now contains solid and liquid phases with separating moving front plan ($x = s$), Stefan wrote two energy equations for the solid and liquid phases in the absence of fluid flow:

$$\rho c_s \frac{\partial T_s}{\partial t} = \frac{\partial}{\partial x} \left(k_s \frac{\partial T_s}{\partial x} \right), 0 \leq x < S(t) \quad (1)$$

$$\rho c_l \frac{\partial T_l}{\partial t} = \frac{\partial}{\partial x} \left(k_l \frac{\partial T_l}{\partial x} \right), S(t) \leq x \quad (2)$$

At the solidification front ($x = S(t)$, & $T_l = T_s = T_m$), the Stefan condition which formulates the energy balance at the interface governs the front velocity:

$$\rho_s \Delta H_m \frac{dS}{dt} \vec{n} = \left[\left(K_s \frac{\partial T}{\partial n} \right)_{x=S(t)} - \left(K_l \frac{\partial T}{\partial n} \right)_{x=S(t)} \right] \vec{n} \quad (3)$$

where \vec{n} is the vector normal to the front directed toward the liquid phase. In addition, for the solidification of pure substances, the temperature condition at the interface is:

$$T_l = T_s = T_m \quad (4)$$

The Stefan problem was to track the moving front position satisfying the interface conditions.

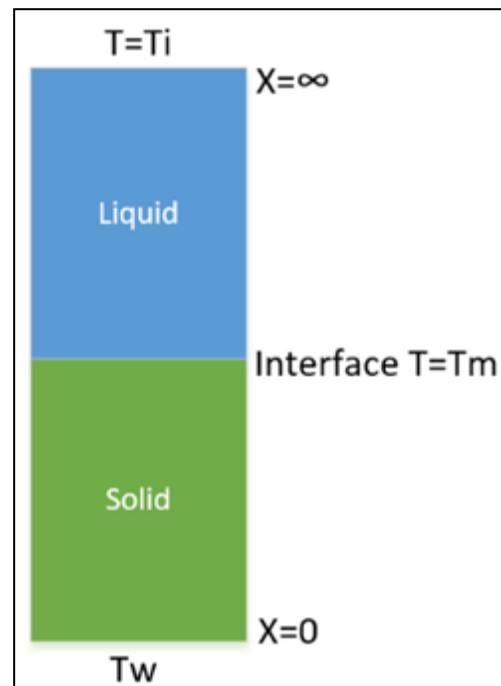


Figure 3. Moving front.

2.2.2. Neumann's Analytical Solution

A one-phase change problem is considered the first and simplest phase change problem; and it applies when, for instance, the liquid is in phase change, while the other phase is at its melting temperature. This type of problem was first analytically solved by Stefan [19]. Stefan's solution assumes constant thermophysical properties in the semi-infinite region to show the rate of melting or solidification.

For a more accurate and practical approach, Neumann formulated Stefan's one-phase solution to be applied to a two-phase problem [14]. In this case, the two-phase in Stefan model becomes a nonlinear model with a moving boundary where the unknowns are the temperature field and the location of the Interface. Taking into consideration that the conservation of energy controls the phase-changing process, the initial state of the PCM is taken to be in the solid phase. Hence, the initial temperature shall be lower than the melting temperature during the melting process and is not kept at a constant value.

The exact analytical solution for the one-dimension Stefan problem is the well-known Neumann solution [10]:

$$S(t) = b\sqrt{t} \quad (5)$$

where the proportionality constant b is the root of the equation:

$$\frac{k_s}{\sqrt{\kappa_s}} \frac{(T_m - T_w)}{\operatorname{erf}\left(\frac{b}{2\sqrt{\kappa_s}}\right)} \exp\left(\frac{-b^2}{4\sqrt{\kappa_s}}\right) - \frac{k_l}{\sqrt{\kappa_l}} \frac{(T_0 - T_m)}{\operatorname{erf}\left(\frac{b}{2\sqrt{\kappa_l}}\right)} \exp\left(\frac{-b^2}{4\sqrt{\kappa_l}}\right) = \rho\Delta H_m \sqrt{\pi} \frac{b}{2} \quad (6)$$

where $\kappa_l = \frac{k_l}{\rho_l c_l}$, $\kappa_s = \frac{k_s}{\rho_s c_s}$.

2.2.3. Model Assumptions

- Heat transfer is dominated by conduction.
- Constant latent heat of fusion/freezing.
- The melting temperature is constant and depends on the nature of the PCM.
- The interface which separates the phases is a sharp front with negligible thickness.

- Thermo-physical properties are different for each phase, which indicates that the thermal conductivities ($k_l \neq k_s$) and the specific heats are not equal as well ($Cp_l \neq Cp_s$)
- Density is considered to be constant ($\rho_l = \rho_s$)
- Super-cooling and nucleation are not present.
- Surface tension is insignificant.
- All the faces are considered to be insulated except for the bottom heat source.
- To explicitly solve the Two-Phase Stefan problem, the slab is assumed to be semi-infinite.
- The presented methodology in this paper is valid only for moving boundary problems in rectangular coordinate problems. There are other systems for the other coordinates.

2.2.4. Governing Equations

Heat conduction equation in one space dimension

$$\rho c T_t = (k T_x)_x \quad (7)$$

$$T_t = \alpha T_{xx} \quad (8)$$

Two-phase Stefan problem, melting of the semi-infinite slab ($0 \leq x < \infty$). Initially solid at ($T_s < T_m$) and with imposing a constant heat source at ($x = 0, T_w > T_m$).

Heat equations for obtaining a change of temperature in liquid and solid phases with time:

$$T_t = \alpha_l T_{xx} \text{ for } (0 < X(t), t > 0) \quad (9)$$

$$T_t = \alpha_s T_{xx} \text{ for } (X(t) < x, t > 0) \quad (10)$$

At the interface ($t > 0$)

$$T(X(t), t) = T_m \quad (11)$$

Stefan condition:

$$\rho h_m X'_{(t)} = -k_l T_x(X(t), t) + k_s T_x(X(t), t) \quad (12)$$

Initial condition:

$$X_{(0)} = 0 \quad (13)$$

$$T_{(x,0)} = T_s \quad (14)$$

Boundary conditions:

$$T_{(0,t)} = T_w \quad (15)$$

$$\lim_{x \rightarrow \infty} T(x, t) = T_s \quad (16)$$

Neumann suggests a solution for this problem to get the position of the melting interface (moving boundary) as shown in the below equations:

$$X_{(t)} = 2\lambda \sqrt{\alpha_l t} \quad (17)$$

The temperature in the liquid region:

$$T_{(x,t)} = T_w - (T_w - T_m) \frac{\operatorname{erf}\left(\frac{x}{2\sqrt{\alpha_l t}}\right)}{\operatorname{erf}\lambda} \quad (18)$$

The temperature in the solid region:

$$T_{(x,t)} = T_s - (T_m - T_s) \frac{\operatorname{erfc}\left(\frac{x}{2\sqrt{\alpha_s t}}\right)}{\operatorname{erfc}(\lambda v)} \quad (19)$$

$$v = \sqrt{\frac{\alpha_l}{\alpha_s}} \quad (20)$$

where the thermal diffusivity for solid and liquid are:

$$\alpha_l = \frac{k_l}{\rho_l c_{p_l}} \quad (21)$$

$$\alpha_s = \frac{k_s}{\rho_s c_{p_s}} \quad (22)$$

We can get λ by solving the transcendental equation below:

$$\frac{St_l}{\exp(\lambda^2) \operatorname{erf}(\lambda)} - \frac{St_s}{v \exp(v^2 \lambda^2) \operatorname{erfc}(v\lambda)} = \lambda \sqrt{\pi} \quad (23)$$

Stefan numbers can be calculated by:

$$St_l = \frac{Cp_l (T_w - T_m)}{h_m} \quad (24)$$

$$St_s = \frac{Cp_s (T_m - T_s)}{h_m} \quad (25)$$

The Newton algorithm is selected to solve the transcendental equation for the Stefan problem to find a unique root lambda. The below equation can be considered to get the first trial for lambda:

$$\lambda = \frac{1}{2} \left[\frac{St_s}{v \sqrt{\pi}} + \sqrt{2 St_l + \left(\frac{St_l}{v \sqrt{\pi}} \right)^2} \right] \quad (26)$$

2.3. Numerical Solution with Apparent Heat Capacity Method

In this work, the apparent heat capacity formulation method for the phase change is selected for solving the problem in the heat conduction process since this method considers the temperature, which is derived from the solution, as the main dependent variable. However, this approach suffers from singularity characteristics in terms of constant temperature phase change problems. Hashemi and Sliepcevich developed a mitigation approach for the singularity problem by assuming that the phase change occurs over a small temperature interval [20].

COMSOL Multiphysics FEM software was used for the numerical modeling of the Stefan problem. Moreover, Smoothed Heaviside step function was successfully used to overcome the singularity problem. The same key assumptions and boundary conditions mentioned in the analytical section above will be numerically tested for the validation against Neumann's analytical solution.

The energy equation for a two-phase system of pure substance is:

$$\left(\frac{\partial}{\partial t} \right) (\rho_1 h_1 \phi_1 + \rho_2 h_2 \phi_2) + \nabla \cdot [(\rho_1 h_1 V_1 + \rho_2 h_2 V_2) + (q_1 \phi_1 + q_2 \phi_2)] - \frac{Dp}{Dt} = 0 \quad (27)$$

$$\phi_1 + \phi_2 = 1 \quad (28)$$

By using Equation (22) in Equation (21)

$$\left(\frac{\partial}{\partial t} \right) [\rho_2 h_2 + (\rho_1 h_1 - \rho_2 h_2) \phi_1] + \nabla \cdot [(\rho_1 h_1 V_1 + \rho_2 h_2 V_2) + \{q_2 + (q_1 - q_2) \phi_1\}] - \frac{Dp}{Dt} = 0 \quad (29)$$

During the phase transition, the phases are at thermal equilibrium, and they are at the same temperature. Hence, the heat transfer is by conduction only, and consequently; Fourier’s equation applies:

$$q = -k\nabla T \tag{30}$$

Then from Equation (23) and Equation (24), the apparent heat capacity formulation is expressed as:

$$\left\{ \frac{\partial(\rho_2 h_2)}{\partial T} + \left[\frac{\partial(\rho_1 h_1)}{\partial T} - \frac{\partial(\rho_2 h_2)}{\partial T} \right] \phi_1 + (\rho_1 h_1 - \rho_2 h_2) \frac{\partial \phi_1}{\partial T} \right\} + \nabla \cdot \{ (\rho_1 h_1 V_1 + \rho_2 h_2 V_2) - [(k_2 + (k_1 - k_2)\phi_1)] \nabla T \} - \frac{Dp}{Dt} = 0 \tag{31}$$

The pressure is assumed to be constant; hence, phases are isotropic and homogeneous. Assuming no motion in the phases. The apparent heat capacity formulation can be simplified to:

$$\rho c \left(\frac{\partial T}{\partial t} \right) = \left(\frac{\partial}{\partial x} \right) \left(k \frac{\partial T}{\partial x} \right) \tag{32}$$

where:

$$\rho_l = \rho_s \tag{33}$$

$$k = k_s + (k_l - k_s)\phi_l \tag{34}$$

$$c = c_s + (c_l - c_s)\phi_l + h_m \frac{d\phi_l}{dt} \tag{35}$$

To calculate the liquid phase fraction for the melting process, and if the transition occurs instantaneously at a constant temperature, then:

$$\phi_l = U(T - T_m) \tag{36}$$

where U is a step function equal to zero if $(T < T_m)$ and one if $(T > T_m)$ as shown in Figure 4a.

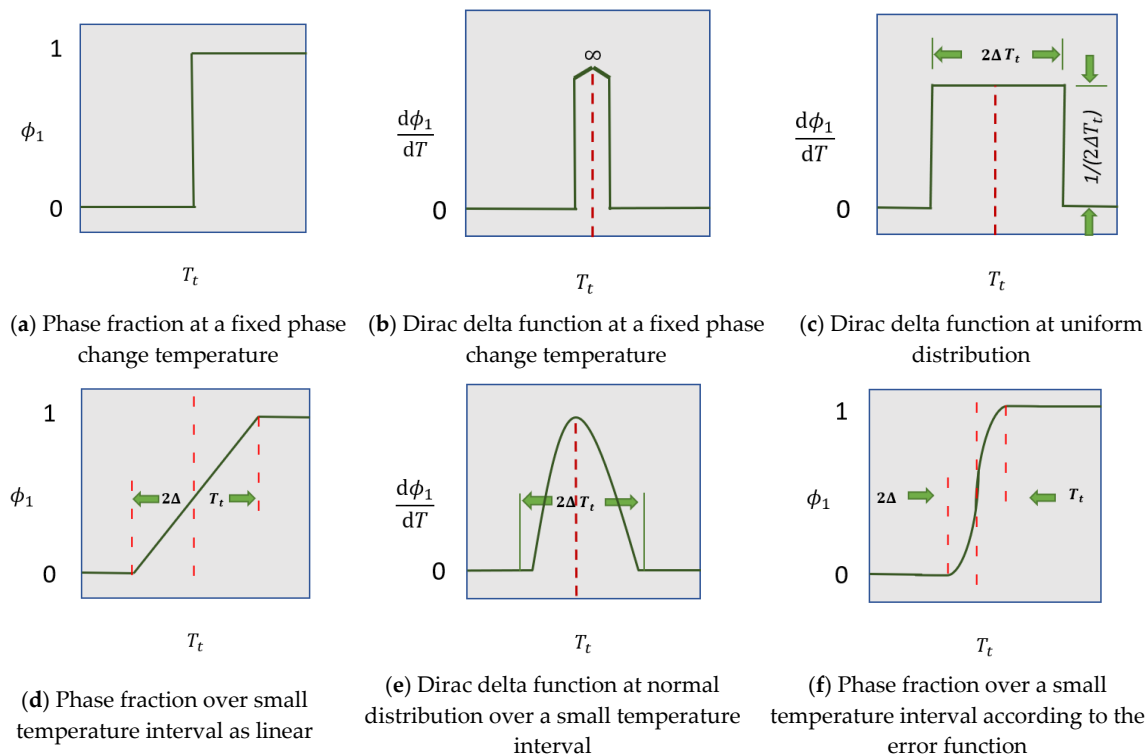


Figure 4. Approximation of sharp melting point with smooth phase transition over a small temperature interval with Dirac Delta and Error Functions.

Variation of the liquid phase fraction with temperature is expressed by the derivation of Equation (30) with temperature Figure 4b:

$$\frac{d\phi_l}{dt} = \delta(T - T_m) \quad (37)$$

To overcome the singularity problem, the Dirac delta function can be approximated as a uniform distribution over a finite temperature interval (Figure 4c,d):

$$\frac{d\phi_l}{dt} = \frac{1}{2\Delta T_m} \quad (38)$$

In the present study smooth variation is assumed as shown in Figure 4e,f as per [20]:

$$\frac{d\phi_l}{dt} = \frac{\epsilon}{\sqrt{\pi}} \exp[-\epsilon^2(T - T_m)^2] \quad (39)$$

The main criterion for the above approach is:

$$\frac{2\Delta T_m}{(T_w - T_m)} < 0.1 \quad (40)$$

3. Test Case: Ice Melting Inside Finite Slab Heated from Below

Heat transfer with phase change has been checked for a simple case “Ice melting in semi-infinite slab” for the sake of verification. Stefan’s problem has been solved analytically by using Neumann approach and was validated numerically using COMSOL Multiphysics to model the transient heat transfer by conduction with phase change. The physical properties and boundary conditions for the test case presented in this study are summarized in Table 1.

Table 1. Test case parameters.

Parameter	Value	Unit
C_{p_l}	4180	[J/kg K]
C_{p_s}	1930	[J/kg K]
k_l	0.598	[W/m K]
k_s	2.2	[W/m K]
ρ_l	1000	[kg/m ³]
ρ_s	1000	[kg/m ³]
h_m	333	[KJ/kg]
T_s	269.15	[K]
T_w	300.15	[K]
T_m	273.15	[K]

4. Results and Discussion

4.1. Analytical and Numerical Solution Analysis

The results have shown a great agreement between the analytical and numerical solutions with an error of less than 0.22% as shown in Figure 5.

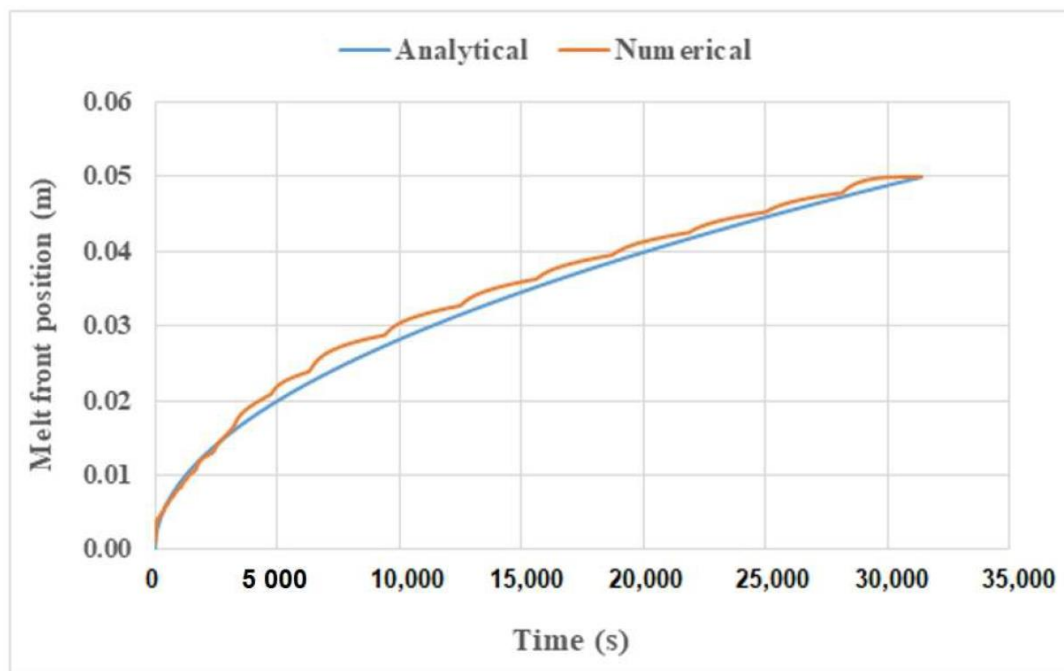


Figure 5. Analytical & Numerical solutions of the melting front position over time.

The evolution of ice temperature along the slab height with respect to time is shown in Figure 6. Here the ice is gradually heated at the bottom wall giving rise to increasing the temperature of the adjacent ice layer and a change in phase from solid to liquid. The latter uses a latent heat formulation, where the latent heat is defined at the melting front, which moves in time. On the micro level, the thermophysical properties of the ice are updated while the heat is transferred from the wall to the ice. At a moment in time, the phase is changed when the ice temperature approaches the transition/melting point. The complete melting occurred after eight hours mainly by the effect of heat conduction.

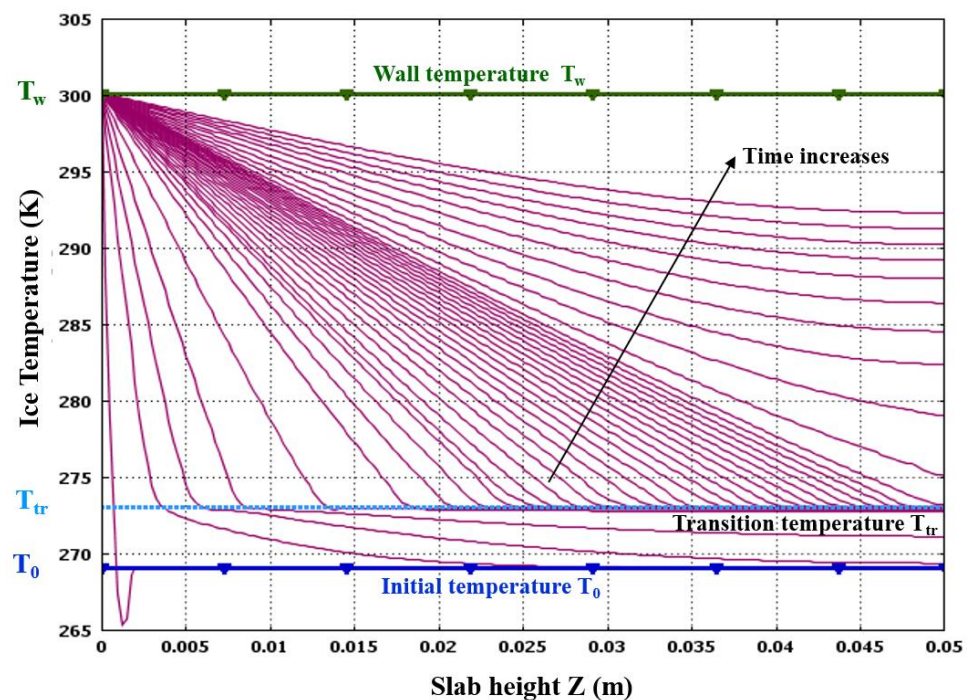


Figure 6. Evolution of ice temperature vs. time along the slab height.

Figure 7 shows the 2-D temperature profile after one (a), three (b), six (c), and nine (d) hours of heating; respectively. The figure gives an example of simulation results and output of postprocessing capabilities in COMSOL. It shows how the melting front moves in space and time in the axial direction along the slab height, as the side and top boundaries are assumed to be adiabatic and, hence; the thermophysical properties are homogeneous in the radial direction. It also shows the increase in temperature within the molten layers and the continuous update of the temperature field with the displacement in the solid front that is changing cautiously with time.

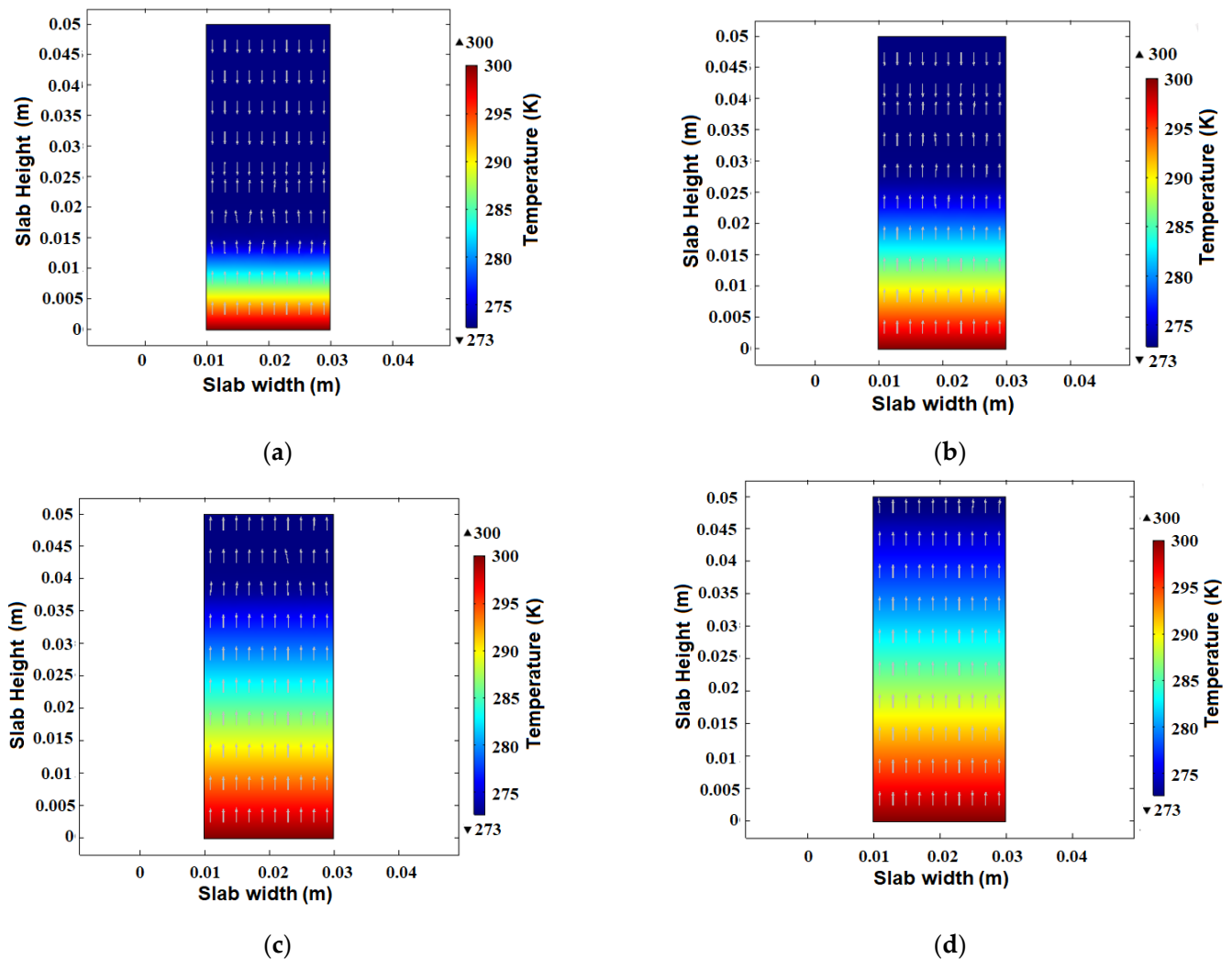


Figure 7. 2D temperature profile along the slab height after one (a), three (b), six (c), and nine (d) hours of heating.

The specific characteristics of phase change and evolution of heat capacity with the temperature at different times and locations along the slab height are further depicted in Figure 8. The phase change is modeled to take place over a mushy region, i.e., narrow temperature interval, rather than a sharp melting point. The plot shows a good coincidence of the heat capacity profile and its peak at different times and locations.

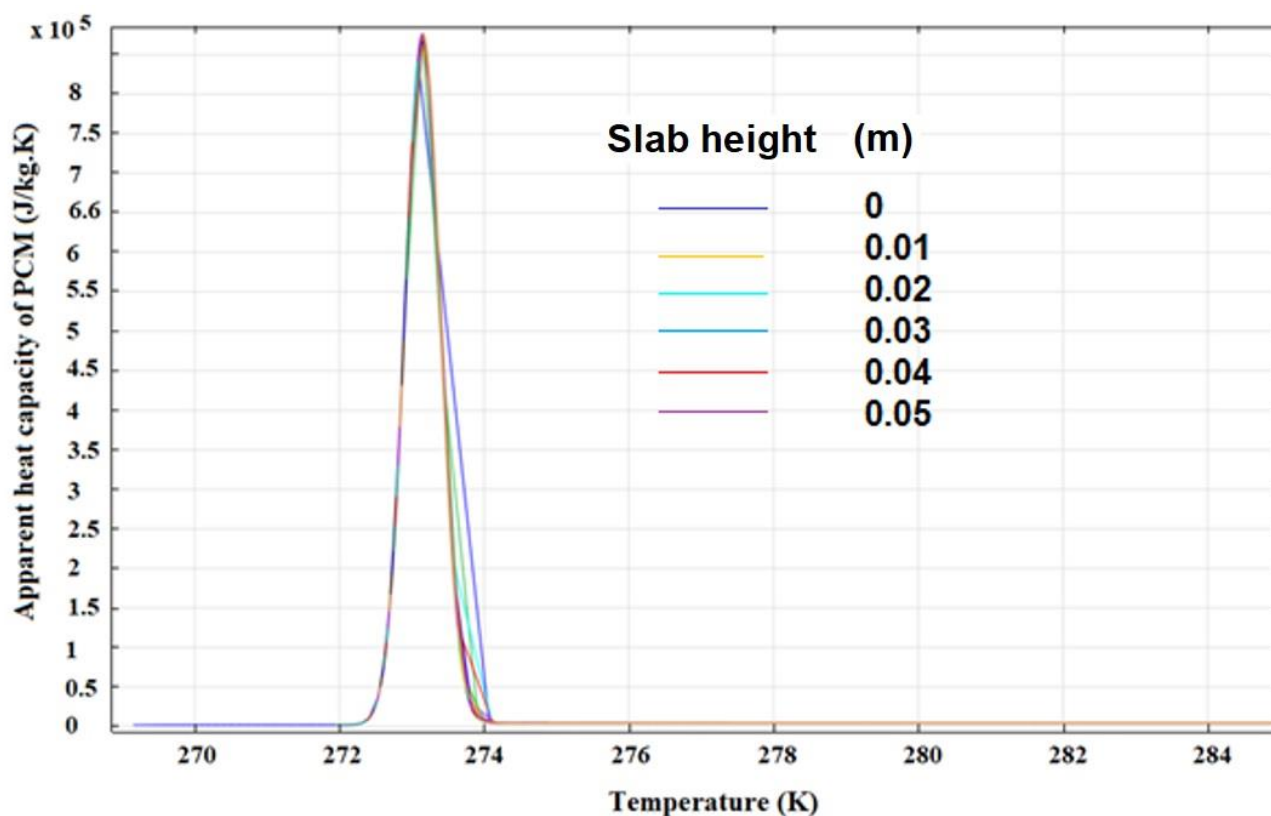


Figure 8. The apparent heat capacity vs. temperature at different times and locations along the slab height.

As an example of the research efforts to examine some of these issues, an improved thermal resistance model has been developed by Ma et al. through applying enhanced conductivity method to incorporate intra PCM convection effects in a 1-D model, with the aim of getting a good compromise between accuracy and simplicity [21]. Their numerical simulation results illustrated that neglecting PCM convective and radiative heat transfer will cause significant errors, which reveals considerable limitations in their model. Similarly, Smitha et al. developed a 1-D simulation model with ambient temperature, irradiance, and wind speed. The simulation model was used to study the effect of varying the PCM melting temperature from 0 °C to 50 °C with the objective of identifying the optimal melting temperature at each geographical location [22]. It has been found that PCM-enhanced cooling is most beneficial in regions with high solar radiation and little seasonal variations in weather conditions. With the optimal PCM melting temperature, the annual PV energy output has increased by over 6% in Mexico and eastern Africa, while over 5% in many locations such as Central and South America, much of Africa, Arabia, Southern Asia and the Indonesian archipelago have been numerically predicted. The research outcomes showed that the increase in energy production varies between 2% and nearly 5% in Europe. It has been, logically, found that higher average ambient temperatures correlate with higher optimal PCM melting temperatures.

4.2. Effect of the Transition Range

It is of interest to examine the effect of the phase transition range on the sensitivity of the apparent heat capacity method. This effect is depicted in Figure 9, where two temperatures, i.e., 0.2 and 2 °K, are arbitrarily selected and compared with the exact analytical solution. It is evident that the error introduced by the difference in the temperature interval is insignificant in the lower region of the domain, which is closer to the interface with the heat source and is more pronounced in the upper part of the domain as the melting front moves in space and time. As the thinner interval conforms more closely to the analytical

solution, it is obvious that the apparent heat capacity formulation can produce accurate predictions. However, for the solar PV passive cooling application, the thicker temperature interval would not have a significant impact on the accuracy. This is valid under the condition that the criterion in Equation (40) is satisfied, i.e., the effect of latent heat variation diminishes as long as the ratio of the temperature range to the overall temperature variation of the PCM is smaller than 0.1.

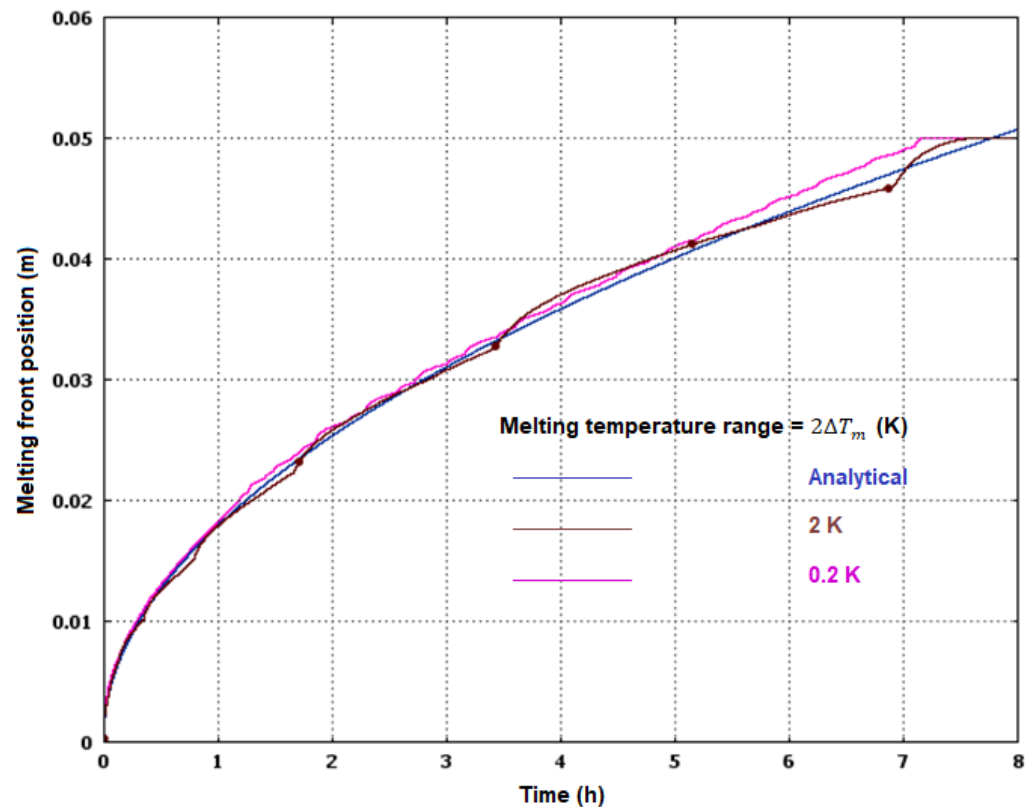


Figure 9. The effect of the melting range on the results' accuracy.

4.3. Effect of the Meshing Quality

With the main goal of reducing the computational time and expenses, the effect of the meshing quality of the numerical simulation on the sensitivity of the apparent heat capacity method is investigated. Three different qualities were used as shown in Figure 10, and the effect on the simulation results is depicted in Figure 11. Similar to the effect of temperature interval, it is evident that the error introduced by the coarser meshing quality is more pronounced in the upper region of the domain and is diminishing in the vicinity of the interface to the heat source.

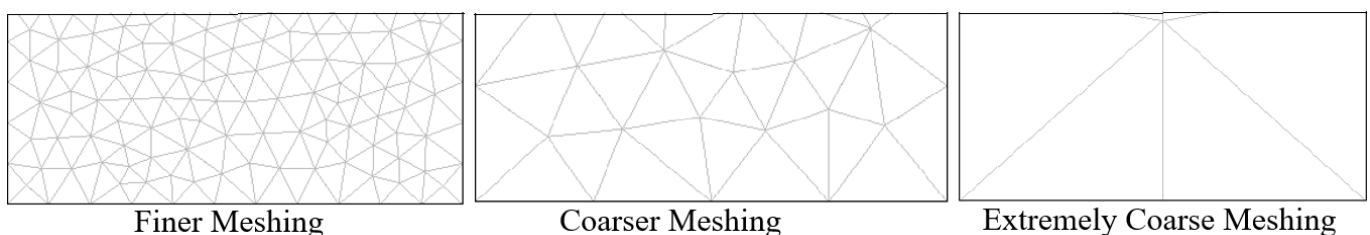


Figure 10. Different meshing qualities.

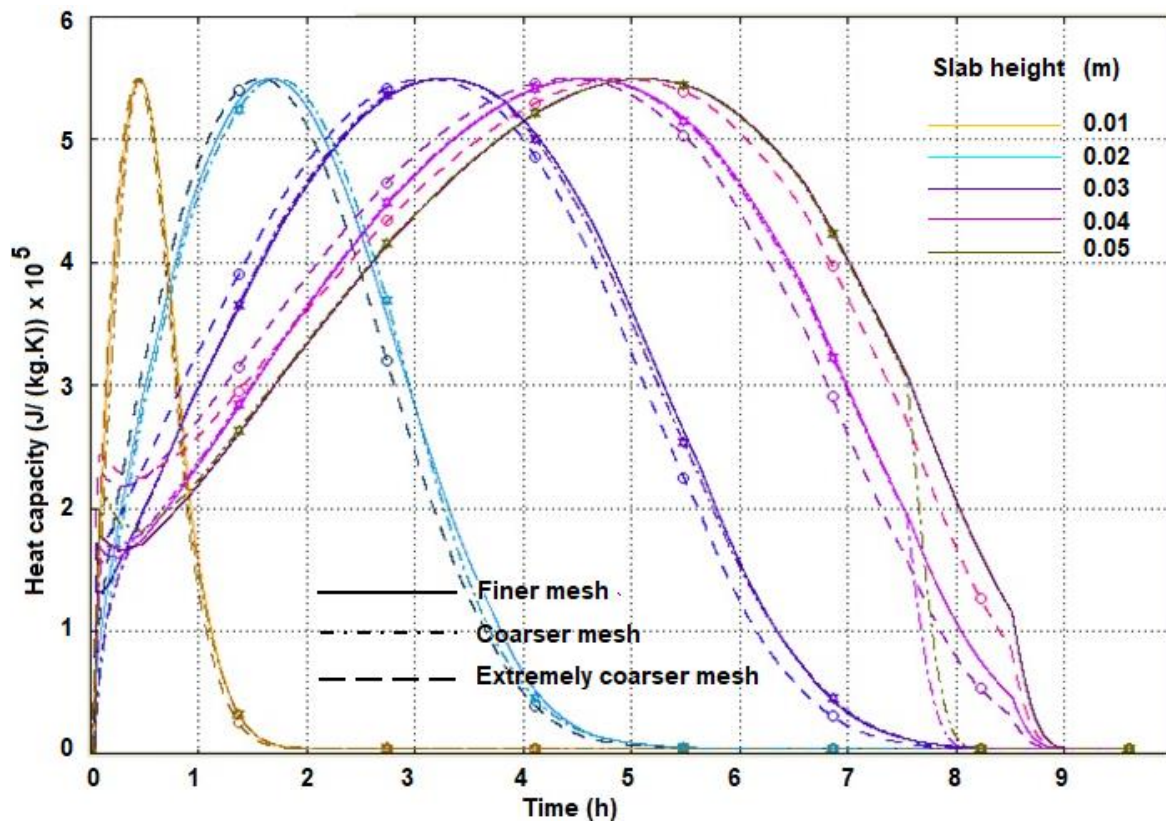


Figure 11. Effect of meshing qualities on the heat capacity.

5. Conclusions

In the present paper, a simulation model for the PCM layer in the PCM Matrix Absorber that is used for passive thermal management of PV modules has been developed and validated against an analytical solution for ice melting in a semi-finite slab. The model neglects intra PCM convection heat transfer and assumes that the solid-liquid phase change takes place over a mushy region rather than a sharp melting temperature. A simplified modeling approach and numerical procedures have been implemented in COMSOL Multiphysics FEM software using the apparent heat capacity formulation and homogenization based on volume averaging techniques. The simulation model has been developed to determine the macroscopic transport and time history of the PCM temperature field, through which the phase change phenomenon can be captured without the need for tracking the melting front during melting and solidification. The model has been validated against a benchmark analytical solution, i.e., Neumann's solution, which was originally developed to solve the classical Stefan Problem.

The simulation results were in good agreement with the results obtained from the analytical solution. The effect of the phase transition range on the sensitivity of the apparent heat capacity method is examined and compared with the exact analytical solution. It is found that the error introduced is insignificant in the lower region of the domain. Moreover, the thinner temperature interval conforms more closely to the exact analytical solution, which is evidence on the accuracy of the apparent heat capacity formulation predictions.

The effect of the meshing quality of the numerical simulation on the sensitivity of the apparent heat capacity method was examined. Similar to the effect of temperature interval, there is evidence that the error introduced by the coarser meshing qualities is diminishing in the close vicinity of the interface with the heat source and more pronounced as the distance from the interface increases.

The simplified model successfully and accurately captures underlying sophisticated physics of phase change problems inside the PCM layer with minimal computational efforts and requires a short convergence time. This simplified and robust model is extremely

important to bridge the large-scale gap between the macroscale level within the PCM layer with moving melting front/solidification front and the length scale of PV modules without the need to track the moving boundary.

Future research utilizing this model can focus on extending the simulation to hybridize the PCM layer with a cellular metallic heat-conducting structure for enhancing its thermal conductivity. The complete model will then be used as a design and optimization tool for performing systematic numerical experiments and sensitivity analysis of PCM-MA under climatic conditions in hot arid areas. The PCM-MA model can then be integrated with the PV panel's model to simulate the complete system of PV passive cooling setup. The complete model will be used as a design and optimization tool for performing systematic numerical experiments and sensitivity analysis that will be discussed comprehensively under climatic conditions in hot regions.

Author Contributions: A.H.: Conceptualization, Methodology, Software, Writing—original draft. Isaifan, R.J.I.: Writing—review & editing. All authors have read and agreed to the published version of the manuscript.

Funding: This research received no external funding.

Data Availability Statement: Data available on request due to privacy restrictions.

Conflicts of Interest: The authors declare that they have no known competing financial interest or personal relationships that could have appeared to influence the work reported in this paper.

Nomenclature

$X_{(t)}$	Interface position [m]
λ	A dimensionless number used in solving Neumann problem
α_l	Liquid thermal diffusivity [m^2/s]
α_s	Solid thermal diffusivity [m^2/s]
t	Time [s]
ρ_l	Density in the liquid phase [Kg/m^3]
ρ_s	Density in solid phase [Kg/m^3]
μ	Viscosity [mPa. S]
k_l	Thermal conductivity in the liquid phase [W/m K]
k_s	Thermal conductivity in solid phase [W/m K]
Cp_l	Heat capacity for liquid phase [J/kg K]
Cp_s	Heat capacity for solid phase [J/kg K]
T_w	Wall temperature [k]
T_m	Melting or transition temperature [K]
T_s	Solid initial temperature [K]
St_l	Stefan Number for liquid phase
St_s	Stefan Number for solid phase
h_m	Latent heat of fusion [J/Kg]
v	Dimensionless number
h	Enthalpy
ϕ	Phase fraction
p	Pressure
q	Heat flux
V	Volumetric flux
k	Thermal conductivity tensor
$\frac{d\phi_l}{dt}$	Dirac delta function

References

- Hassabou, A.H.; Abdallah, A.A.; Abotaleb, A. Passive Cooling of Photovoltaic Modules in Qatar by Utilizing PCM-Matrix Passive Cooling of Photovoltaic Modules in Qatar by Utilizing PCM- Matrix Absorbers. *ISES Sol. World Congr.* **2019**. [\[CrossRef\]](#)
- Fares, E.; Buffiere, M.; Figgis, B.; Haik, Y.; Isaifan, R.J. Soiling of photovoltaic panels in the Gulf Cooperation Council countries and mitigation strategies. *Sol. Energy Mater. Sol. Cells* **2021**, *231*, 111303. [\[CrossRef\]](#)

3. Fares, E.; Aissa, B.; Isaifan, R.J. Inkjet printing of metal oxide coatings for enhanced photovoltaic soiling environmental applications. *Glob. J. Environ. Sci. Manag.* **2022**, *8*, 1–18. [[CrossRef](#)]
4. Kern, J.E.C.; Russell, M.C. Combined Photovoltaic and Thermal Hybrid Collector Systems. In Proceedings of the 13th Photovoltaic Specialists Conference, Washington, DC, USA, 5–8 June 1978; pp. 1153–1157.
5. Chow, T.T. A review on photovoltaic/thermal solar technology. *Appl. Energy* **2010**, *87*, 365–379. [[CrossRef](#)]
6. Hasan, M.A.; Sumathy, K. Photovoltaic thermal module concepts and their performance analysis. *Renew. Sustain. Energy Rev.* **2010**, *14*, 1845–1859. [[CrossRef](#)]
7. Zhang, X.; Zhao, X.; Smith, S.; Xu, J.; Yu, X. Renew of R&D progress and practical application of teh solar photovoltaic/ thermal (PV/T) technologies. *Renew. Sustain. Energy Rev.* **2012**, *16*, 599–617.
8. Ahmad, A.; Navarro, H.; Ghosh, S.; Ding, Y.; Roy, J.N. Evaluation of New PCM/PV Configurations for Electrical Energy Efficiency Improvement through Thermal Management of PV Systems. *Energies* **2021**, *14*, 4130. [[CrossRef](#)]
9. Isaifan, R.J.; Johnson, D.; Ackermann, L.; Figgis, B.; Ayoub, M. Evaluation of the adhesion forces between dust particles and photovoltaic module surfaces. *Sol. Energy Mater. Sol. Cells* **2019**, *191*, 413–421. [[CrossRef](#)]
10. Faraj, K.; Khaled, M.; Faraj, J.; Hachem, F.; Castelain, C. Phase change material thermal energy storage systems for cooling applications in buildings: A review. *Renew. Sustain. Energy Rev.* **2020**, *119*, 109579. [[CrossRef](#)]
11. Akbari, S. Dust storms, sources in the Middle East and economic model for survey it's impacts. *Aust. J. Basic Appl. Sci.* **2011**, *5*, 227–233.
12. Choubineha, N.; Jannesarib, H.; Kasaeian, A. Experimental study of the effect of using phase change materials on the performance of an air-cooled photovoltaic system. *Renew. Sustain. Energy Rev.* **2019**, *101*, 103–111. [[CrossRef](#)]
13. Adibpour, S.; Raisi, A.; Ghasemi, B.; Sajadi, A.R.; Rosengarten, G. Experimental investigation of the performance of a sun tracking photovoltaic panel with phase change material. *Renew. Energy* **2021**, *165*, 321–333. [[CrossRef](#)]
14. Neumannn, F. Die Paruellen Differentialgleichungen der Mathematischen Physik. *Mon. Für Math. Und Phys.* **1912**, *23*, A49. [[CrossRef](#)]
15. Kroeger, P.; Ostrach, S. The solution of a two-dimensional freezing problem including convection effects in the liquid region. *Int. J. Heat Mass Transf.* **1973**, *17*, 1191–1207. [[CrossRef](#)]
16. Mori, A.; Araki, K. Methods for analysis of the moving boundary surface problem. *Int. Chem. Eng.* **1976**, *16*, 734.
17. Voller, V. An Overview of Numerical Methods for Solving Phase Change Problems. In *Advances in Numerical Heat Transfer*; Minkowycz, W.J., Sparrow, E.M., Eds.; John Wiley & Sons, Ltd.: Hoboken, NJ, USA, 1997.
18. Civan, F.; Sliepcevuch, C. Limitation in the apparent heat capacity formulation for heat transfer with phase change. *Proc. Okla. Acad. Sci.* **1987**, *67*, 83–89.
19. Stefan, J. Stefan Number. *S B Wien. Akad. Mat. Natur.* **1889**, *98*, 473–484 + 965–983.
20. Hashemi, H.; Sliepcevich, C. The heat pipe. *Chem. Eng. Prog. Symp. Ser.* **1967**, 34–41.
21. Ma, T.; Zhao, J.; Li, Z. Mathematical modelling and sensitivity analysis of solar photovoltaic panel integrated with phase change material. *Appl. Energy* **2018**, *228*, 1147–1158. [[CrossRef](#)]
22. Smitha, C.J.; Forsterb, P.; Crooka, R. Global analysis of photovoltaic energy output enhanced by phase change material cooling. *Appl. Energy* **2014**, *126*, 21–28. [[CrossRef](#)]